Electronic Supplementary Material (ESI) for Nanoscale Advances.
This journal is © The Royal Society of Chemistry 2023

Electronic Supplementary Information

Au@C/Pt Core@Shell/Satellites Supra-Nanostructures: Plasmonic Antenna-Reactor Hybrid Nanocatalysts

Zixin Wang and Hui Wang*

Department of Chemistry and Biochemistry, University of South Carolina, Columbia, South Carolina 29208, United States

* Corresponding author.

Email: wang344@mailbox.sc.edu (H. Wang); Phone: 1-803-777-2203; Fax: 1-803-777-9521; orcid.org/0000-0002-1874-5137.

S1. Additional Experimental Details

S1.1 Chemicals and Materials

Gold(III) chloride trihydrate ($HAuCl_4 \cdot 3H_2O$, ACS grade), polyvinylpyrrolidone (PVP, average molecular weight: 58,000), ethylene glycol (EG), and tetraethylene glycol (TEG) were purchased from Alfa Aesar. Hydrochloric acid (HCl, 1.0 M), sodium citrate dihydrate, sodium phosphate monobasic (NaH_2PO_4), sodium phosphate dibasic (Na_2HPO_4), and ethanol (200 proof) were purchased from Fisher Scientific. Potassium tetrachloroplatinate (K_2PtCl_4, reagent grade, 98 %), trizma base (TB, >99.0%), nickel nitrate hexahydrate ($Ni(NO_3)_2 \cdot 6H_2O$), and Nafion perfluorinated resin solution (5 wt %) were purchased from Sigma Aldrich. 3,3′,5,5′-Tetramethylbenzidine (TMB) was purchased from SeraCare Life Sciences. All reagents were used as received without further purification. Ultrapure Milli-Q water (18.2 MΩ resistivity, Millipore) was used for all experiments.

S1.2 Synthesis of Au Nanoparticles

Colloidal Au nanoparticles with controlled sizes were synthesized following a previously reported protocol.[1] To synthesize Au nanoparticles with an average diameter of 17 nm, 0.5 mL of 25 mM $HAuCl_4$ was first added into 48 mL of boiling water under magnetic stir. After continuously stirring the solution for 10 min, 1.5 mL of 1 w/w % sodium citrate was added into the boiling mixture, which was stirred and refluxed for 30 min before cooling down to room temperature. The resulting Au colloids (~ 17 nm in diameter) were then used as the seeds to grow Au nanoparticles with an average diameter of ~ 40 nm. 4 mL of Au seeds were reacted with 75 μmol of $HAuCl_4$ in 200 mL of 4 mM TB buffer at the boiling temperature (~ 100 ^oC) for 30 min. After cooling down to room temperature, the resulting colloidal Au nanoparticles were centrifuged, washed with water through 3 cycles of redispersion/centrifugation, and finally resuspend in 10 mL of water for storage. Larger Au nanoparticles with an average diameter of ~ 114 nm were synthesized by reacting 80 μL of colloidal Au nanoparticles (40 nm in diameter) with 50 μmol of $HAuCl_4$ in 100 mL of 4 mM TB buffer at the boiling temperature for 30 min. After cooling down to room temperature, the resulting colloidal Au nanoparticles were centrifuged, washed with water through 3 cycles of redispersion/centrifugation, and finally resuspend in 1 mL of water for storage and future use.

S1.3 Synthesis of Au@Ni_3C Core@Shell Nanoparticles

Au@Ni_3C core@shell nanoparticles were synthesized by growing Ni_3C shells on Au cores through a polyol-mediated process.[2] Briefly, 300 μL of the stock suspension of colloidal Au nanoparticles (average diameter of ~ 114 nm) were mixed with 100, 300, or 600 μL of 10 mM $Ni(NO_3)_2$ (dissolve in TEG) in a 5 mL of TEG containing 1 w/w % PVP. The reactant mixtures were boiled at 300 ^oC for 6 min. The resulting colloidal nanoparticles were quickly cooled in an ice bath, centrifuged, washed with ethanol through 3 cycles of redispersion/centrifugation, and finally redispersed in 1.8 mL of ethanol for storage. The thickness of the Ni_3C shells increased with the amount of $Ni(NO_3)_2$ in the reactant mixtures.

S1.4 Synthesis of Au@C Core@Shell Nanoparticles

Au@C core@shell nanoparticles were synthesized by selectively etching Ni in the Au@Ni_3C core@shell nanoparticles with an etchant solution containing 0.5 M HCl for 12 h at room temperature.

The resulting Au@C core@shell nanoparticles were centrifuged, washed with water through 3 cycles of redispersion/centrifugation, and finally redispersed in 1 mL of water for storage and future use.

S1.5 Etching the Au Cores of Au@C Core@Shell Nanoparticles

The Au cores could be selectively etched at room temperature by exposing the Au@C core@shell nanoparticles to an etchant solution containing 0.34 mM I_2 and 2.0 mM KI.[3] Completely etching of the Au cores was accomplished typically after 2 h, resulting in the formation of spherical C nanoshells with hollow interiors.

S1.6 Nanostructure Characterizations

The particle sizes and morphologies of the nanostructures were characterized by transmission electron microscopy (TEM) using a Hitachi HT-7800 transmission electron microscope operated at an accelerating voltage of 120 kV. To prepare samples for TEM imaging, colloidal particles dispersed in water were drop-cast and dried on 300 mesh Formvar/carbon-coated Cu grids (Electron Microscopy Science Inc.) at room temperature. The Pt/Au atomic ratios of various Au@C/Pt samples were quantified through energy dispersive spectroscopy (EDS)-based elemental analysis using an EDS analysis unit attached to the Hitachi HT-7800 transmission electron microscope. Powder X-ray diffraction (PXRD) patterns were recorded on a SAXSLab Ganesha (Cu Kα = 1.5406 Å) using the off-axis wide-angle X-ray scattering mode. Optical extinction spectra of colloidal nanoparticles suspended in water were collected at room temperature using a Beckman Coulter Du 640 spectrophotometer. X-ray photoelectron spectroscopy (XPS) measurements were carried out using a Krato AXIS Ultra DLD XPS system equipped with a monochromatic Al Kα source. The sample for XPS measurements was dried in vacuum on a Si wafer (University Wafer, Inc.) before being loaded into the XPS chambers. Electrochemical impedance spectroscopy (EIS) measurements were performed using a CHI660E electrochemistry workstation (CH Instruments, Austin, Texas) at room temperature with a three-electrode system, in which a Pt wire served as the counter electrode, a saturated calomel electrode (SCE) served as the reference, and a nanoparticle-loaded glassy carbon electrode (GCE, 3 mm diameter) served as the working electrode, respectively. The GCE was polished with 0.3 μm alumina slurry and then washed thoroughly with water and ethanol. 1 μL of colloidal ink of Au, Au@C, or Au@C/Pt nanoparticles (all containing 100 μg of Au in 1 mL of ink) were drop-cast on a pretreated GCE and dried in air at room temperature. Then 2 μL of Nafion perfluorinated resin solution (0.2 wt %) was drop-dried on the electrode surface to hold the nanoparticles. The EIS results were collected in 0.4 M KCl supporting electrolyte containing 0.5 mM $K_3Fe(CN)_6$ and 0.5 mM $K_4Fe(CN)_6$, using an alternating current voltage of 5.0 mV within the frequency range from 1×10^{-2} to 1×10^5 Hz.

S2. Additional Figures

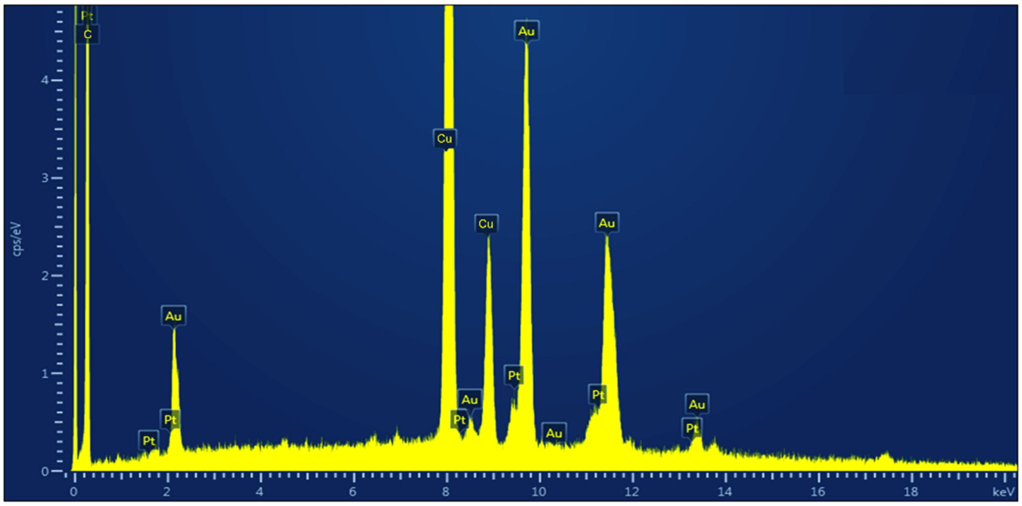

Figure S1. Energy dispersive spectrum of Au@C/Pt nanohybrids synthesized by reacting Au@C core@shell nanoparticles (Au core size: 114 ± 6.3 nm; C shell thickness: 20.4 ± 2.4 nm) with 300 µM of K_2PtCl_4. This sample was labeled as Au@C/Pt-3, as listed in Table 1 in the main text. The Cu signals in the spectrum were from the Cu grid used for TEM imaging.

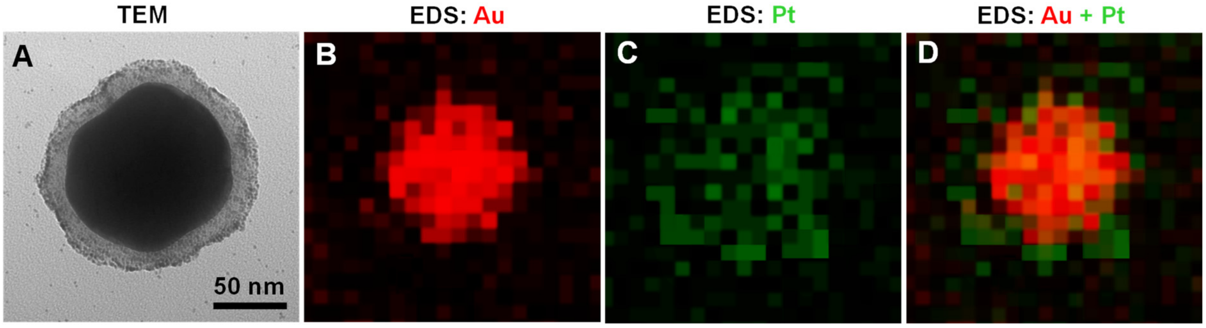

Figure S2. (A) TEM image and EDS elemental maps of (B) Au, (C) Pt, and (D) overlaid Au + Pt of an individual Au@C/Pt particle. This sample was labeled as Au@C/Pt-3, as listed in Table 1 in the main text. Because of the presence of both C and Cu in the TEM grid, the EDS signals of Cu and C were not utilized for the elemental mapping measurements.

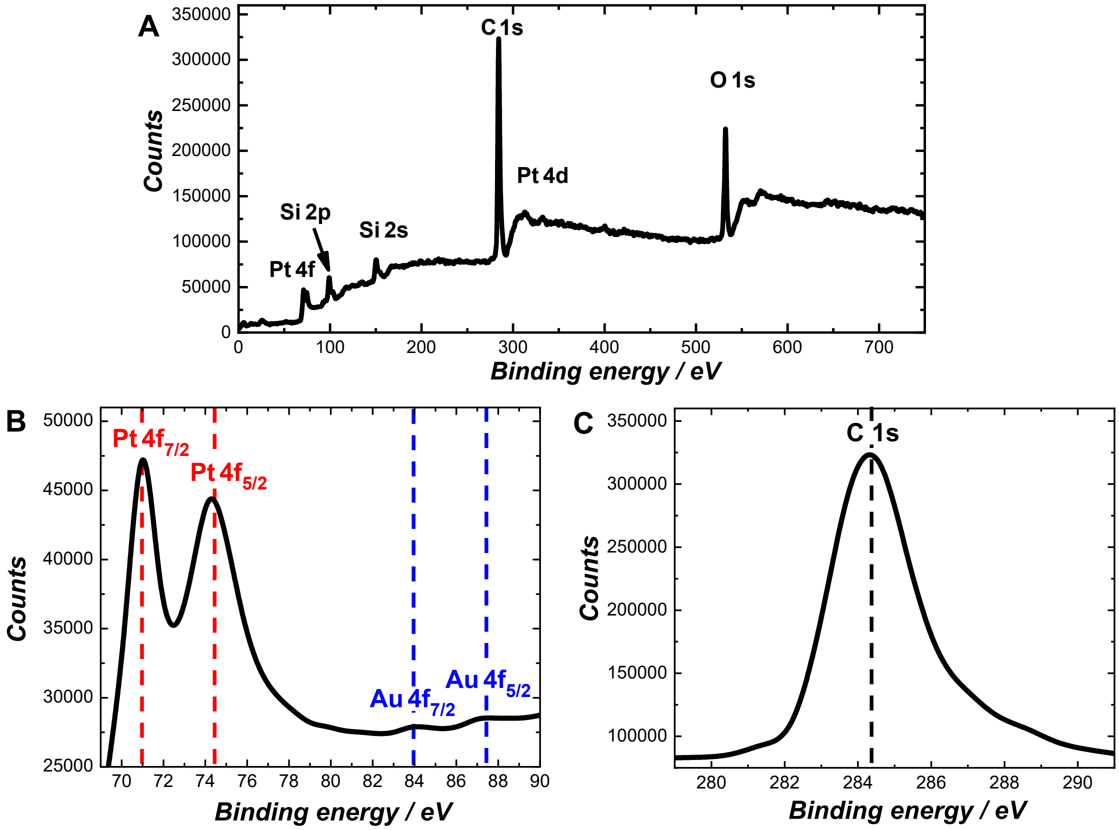

Figure S3. XPS results collected from Au@C/Pt-3 on a Si substrate: (A) Wide survey spectrum, (B) spectrum in the Pt 4f and Au 4f region, and (C) spectrum in the C 1s region.

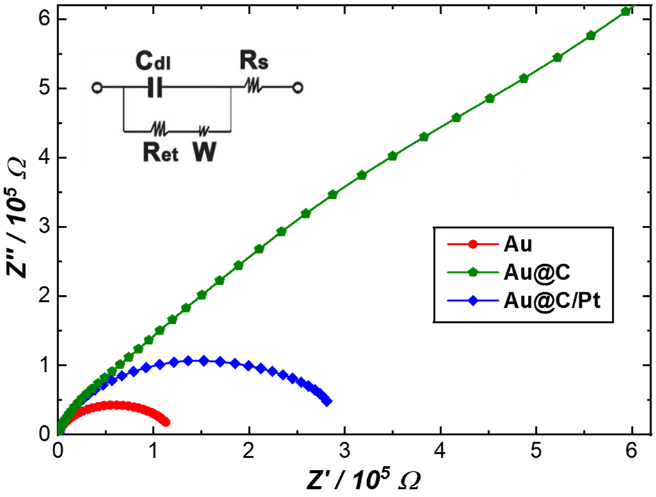

Figure S4. Nyquist diagrams of electrochemical impedance spectra (EIS) recorded in an electrolyte containing 0.5 mM $[Fe(CN)_6]^{3-}$, 0.5 mM $[Fe(CN)_6]^{4-}$, and 0.4 M KCl using a GCE loaded with Au, Au@C-2, or Au@C/Pt-3 as the working electrode. The inset shows the equivalent circuit used to fit the EIS data.

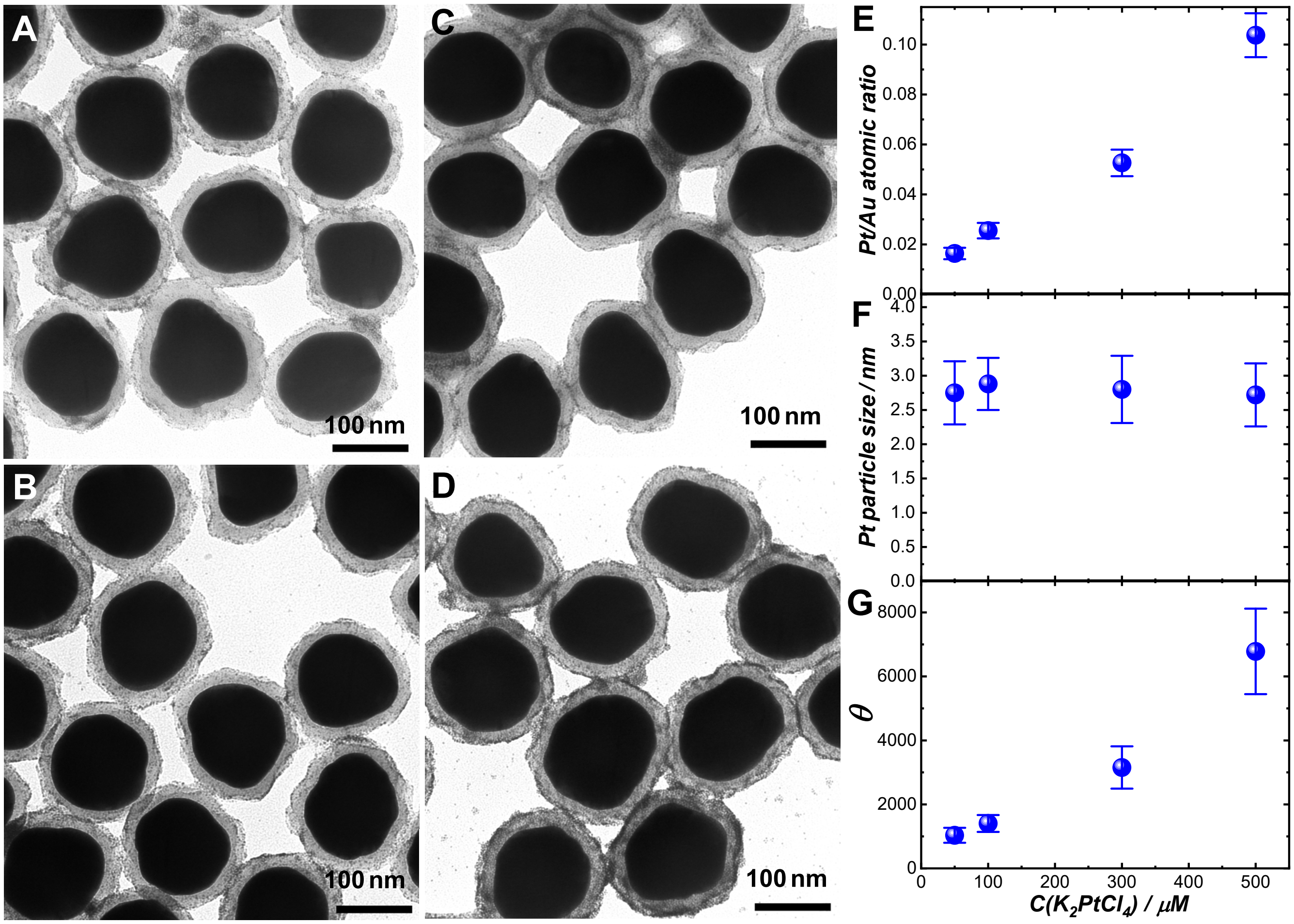

Figure S5. TEM images of Au@C/Pt nanohybrids synthesized by reacting Au@C core@shell nanoparticles (Au core size: 114 ± 6.3 nm; C shell thickness: 20.4 ± 2.4 nm) with (A) 50, (B) 100, (C) 300, and (D) 500 μM of K_2PtCl_4. The samples shown in panels A, B, C, and D were labeled as Au@C/Pt-1, Au@C/Pt-2, Au@C/Pt -3, and Au@C/Pt-4, respectively, as listed in Table 1 in the main text. (E) Relationship between the Pt/Au atomic ratio in the Au@C/Pt nanocatalysts (quantified by EDS) and the initial concentration of K_2PtCl_4 in the reactant mixtures. (F) Relationship between Pt particle size in the Au@C/Pt nanocatalysts and the initial concentration of K_2PtCl_4 in the reactant mixtures. (G) Relationship between θ (defined as the average number of Pt nanoparticles on each Au@C core@shell particle) and the initial concentration of K_2PtCl_4 in the reactant mixtures. The values of θ were calculated based on the Pt/Au atomic ratio (quantified by EDS), the molar masses of Pt (195 g mol^{-1}) and Au (197 g mol^{-1}), mass densities of Pt (21.4 g cm^{-3}) and Au (19.3 g cm^{-3}), and the volumes of Au and Pt nanoparticles. The particle volumes of Au and Pt were calculated assuming a spherical shape using the particle diameters extracted from TEM images.

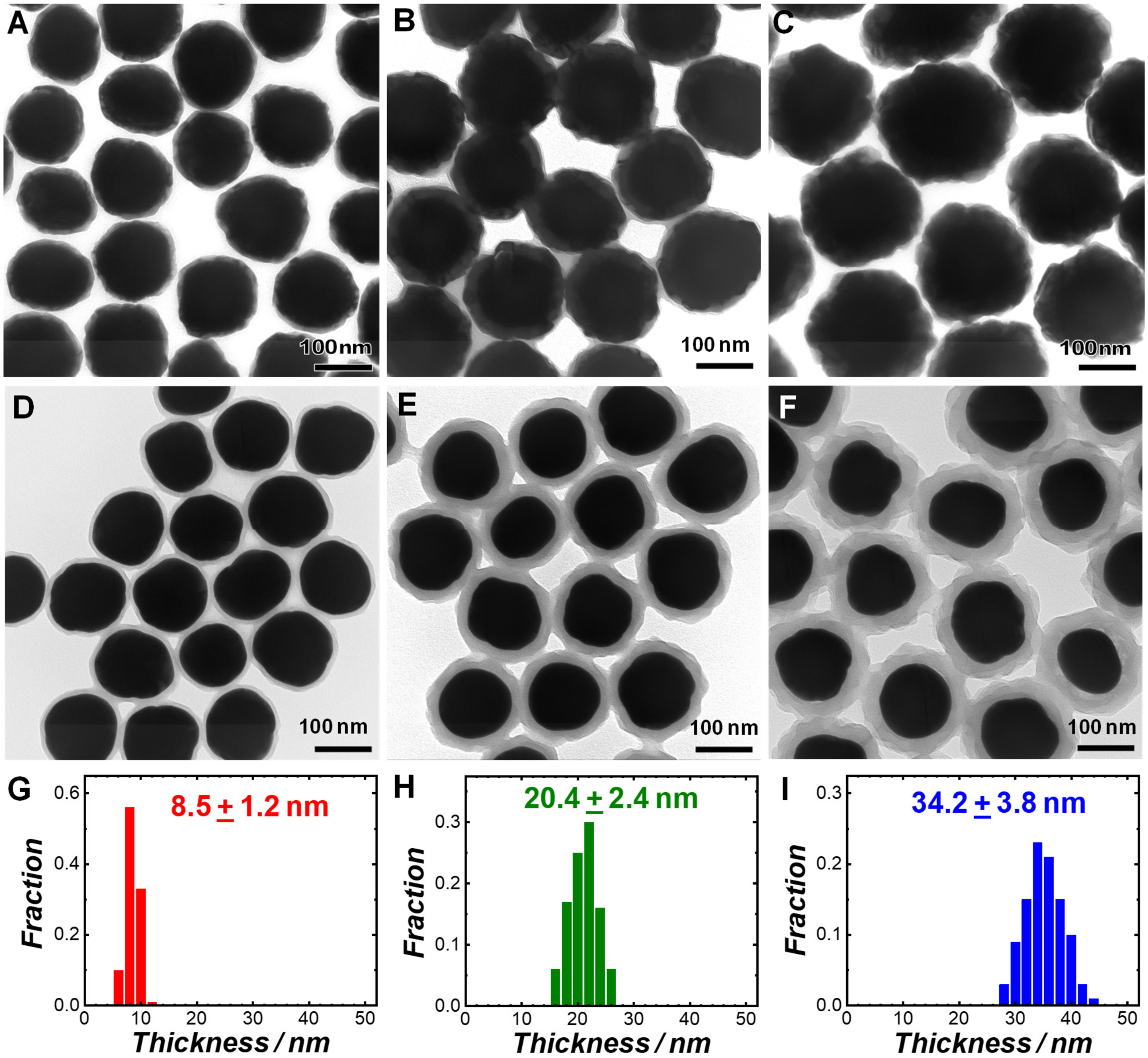

Figure S6. (A-C) TEM images of Au@Ni_3C core@shell nanoparticles with a core size of 114 ± 6.3 nm and various shell thicknesses. The Au@Ni_3C core@shell nanoparticles were synthesized by reacting Au nanoparticles with (A) 0.20, (B) 0.60, and (C) 1.2 mM $Ni(NO_3)_2$, respectively. TEM images of (D) Au@C-1, (E) Au@C-2, and (F) Au@C-3 core@shell nanoparticles, which were derived from the Au@Ni_3C core@shell nanoparticles shown in panels A, B, and C, respectively. Distribution of C shell thicknesses in (G) Au@C-1, (H) Au@C-2, and (I) Au@C-3.

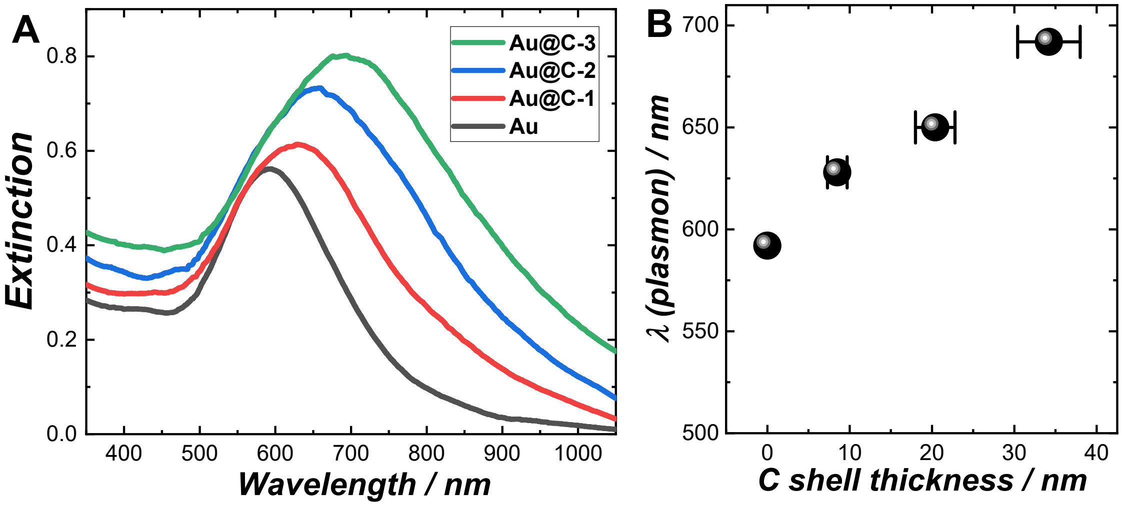

Figure S7. (A) Optical extinction spectra of colloidal Au nanoparticles (114 ± 6.3 nm), Au@C-1 (Au core size: 114 ± 6.3 nm; C shell thickness: 8.5 ± 1.2 nm), Au@C-2 (Au core size: 114 ± 6.3 nm; C shell thickness: 20.4 ± 2.4 nm), and (C) Au@C-3 (Au core size: 114 ± 6.3 nm; C shell thickness: 34.8 ± 3.8 nm). All colloidal samples had nominally the same Au mass concentration of 21.3 mg L^{-1}. (B) Relationship between the plasmon resonance wavelength, λ(plasmon), and C shell thickness.

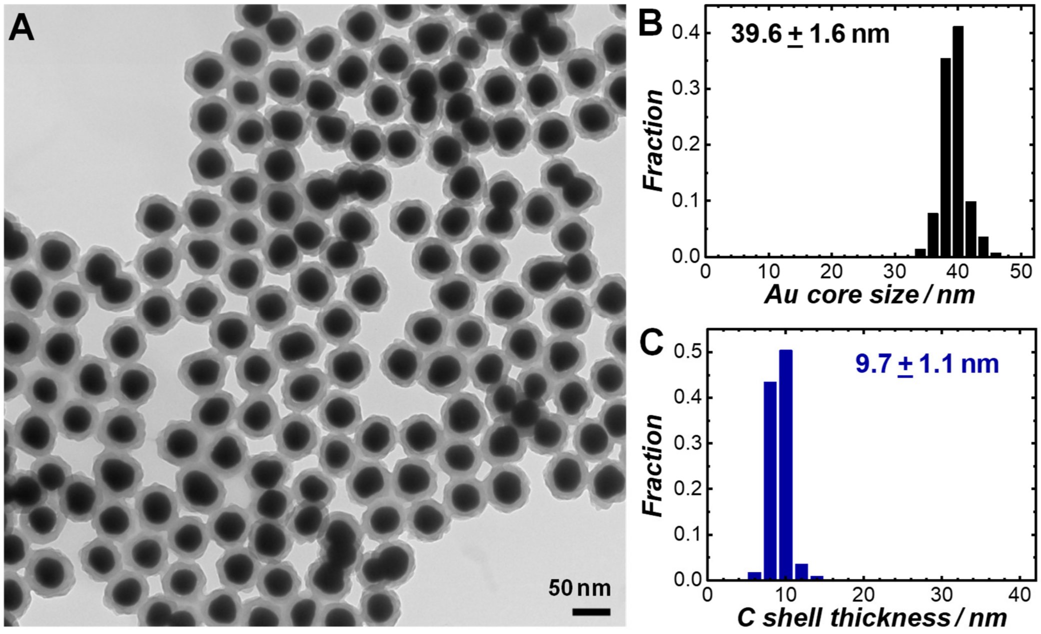

Figure S8. (A) TEM image, (B) Au core size distribution, and (C) C shell thickness distribution of an Au@C core@shell nanoparticle sample synthesized using 39.6 nm Au nanoparticles as the cores.

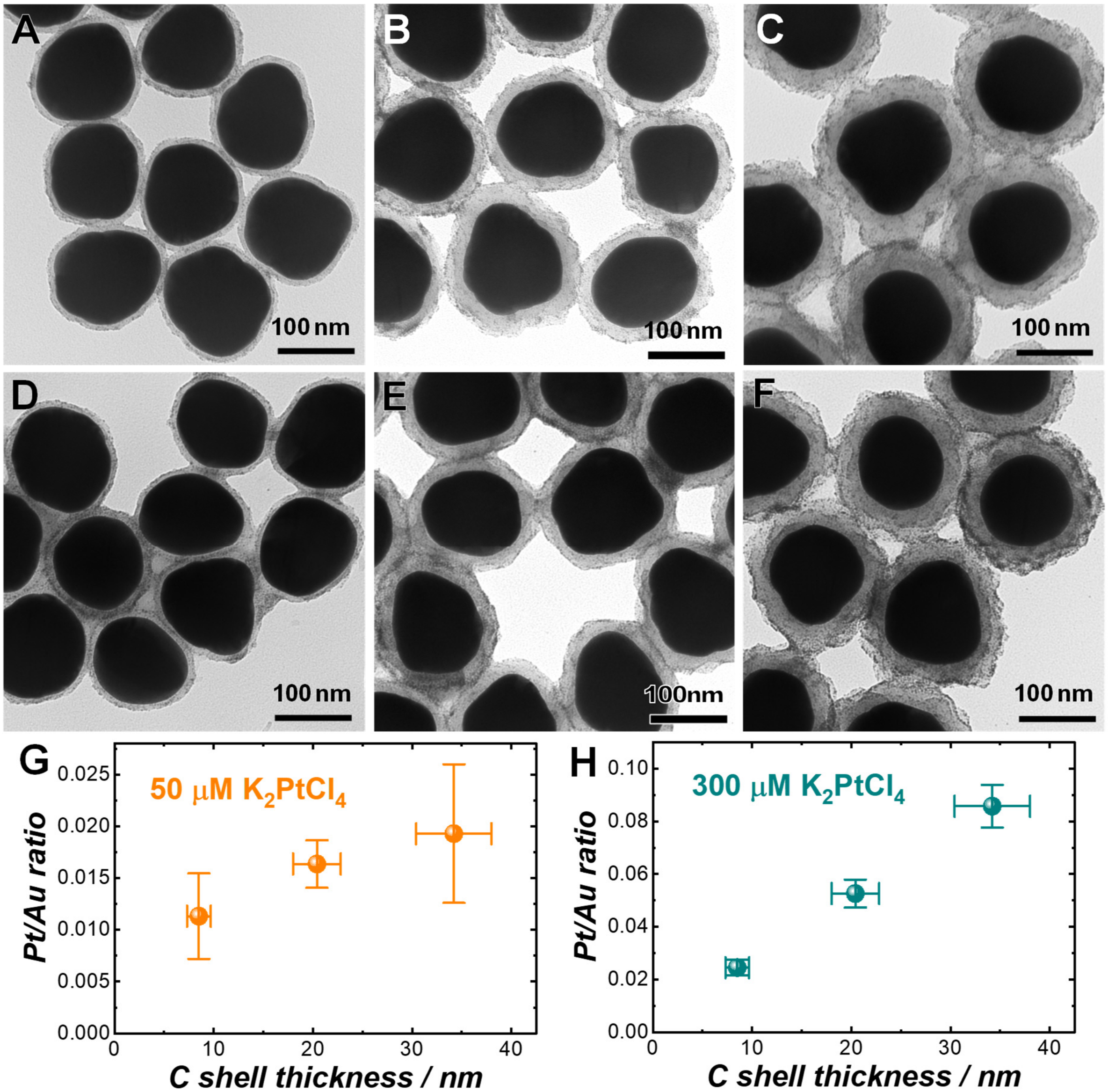

Figure S9. TEM images of Au@C/Pt nanohybrids synthesized by reacting (A) Au@C-1 with 50 μM of K_2PtCl_4, (B) Au@C-2 with 50 μM of K_2PtCl_4, (C) Au@C-3 with 50 μM of K_2PtCl_4, (D) Au@C-1 with 300 μM of K_2PtCl_4, (E) Au@C-2 with 300 μM of K_2PtCl_4, and (F) Au@C-3 with 300 μM of K_2PtCl_4. The samples shown in panels A, B, C, D, E, F, and G were labeled as Au@C/Pt-7, Au@C/Pt-1, Au@C/Pt-8, Au@C/Pt-5, Au@C/Pt-3, and Au@C/Pt-6, respectively, as listed in Table 1 in the maintext. Pt/Au atomic ratios of Au@C/Pt samples with various C shell thicknesses synthesized at K_2PtCl_4 concentrations of (G) 50 and (H) 300 μM.

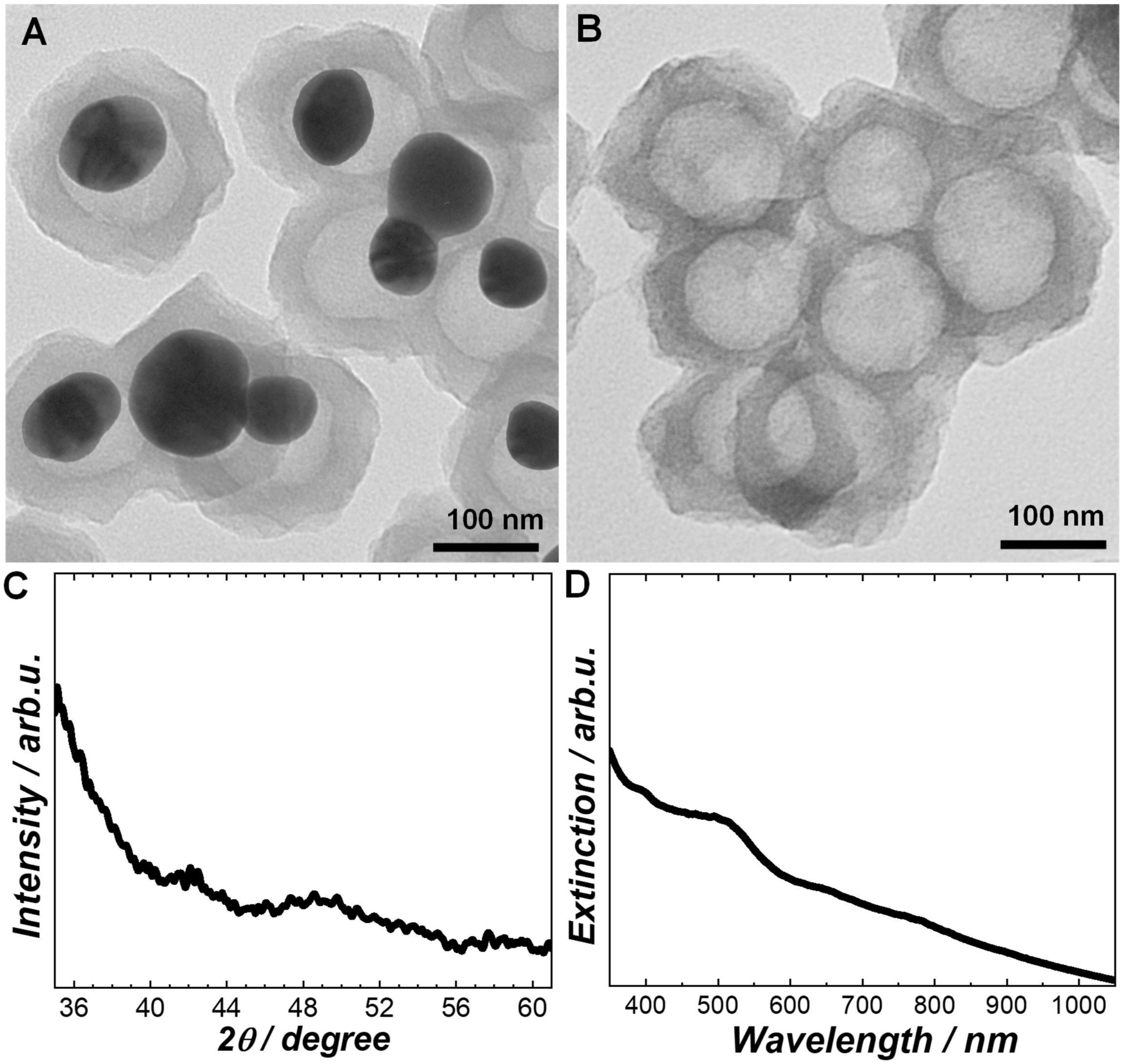

Figure S10. TEM image of Au@C-3 core@shell nanoparticles (Au core size: 114 ± 6.3 nm; C shell thickness: 34.8 ± 3.8 nm) after exposure to an etchant solution containing 0.34 mM I_2 and 2.0 mM KI for (A) 0.5 h and (B) 3 h at room temperature. (C) PXRD pattern and (D) optical extinction spectrum of C nanoshells synthesized after complete etching of the Au cores in the Au@C-3 (3 h etching).

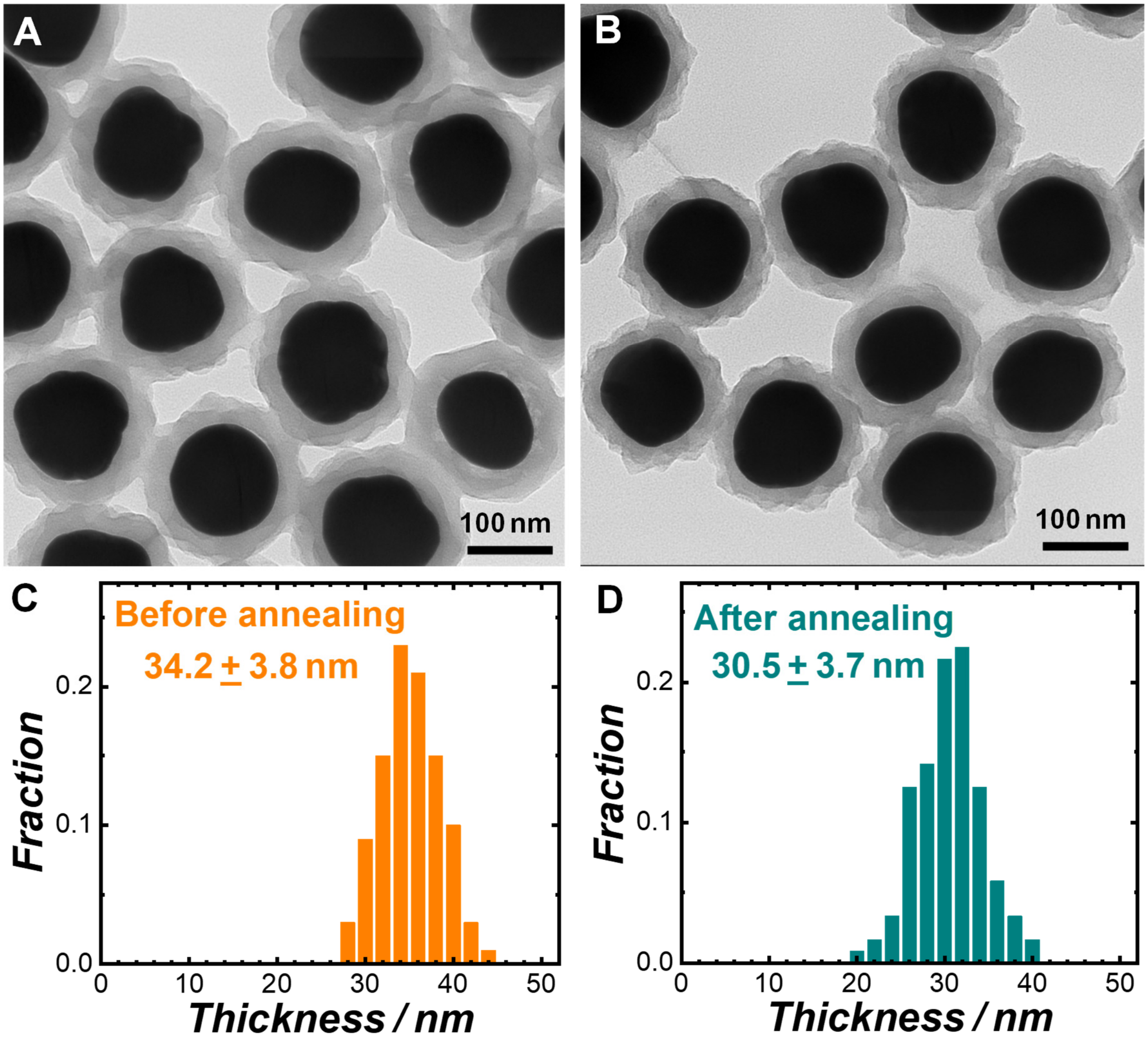

Figure S11. TEM images of Au@C-3 core@shell nanoparticles (A) before and (B) after thermal annealing at 450 ºC in an N_2 atmosphere for 2 h. Distributions of C shell thicknesses for Au@C-3 (C) before and (D) after annealing at 450 ºC in an N_2 atmosphere for 2 h.

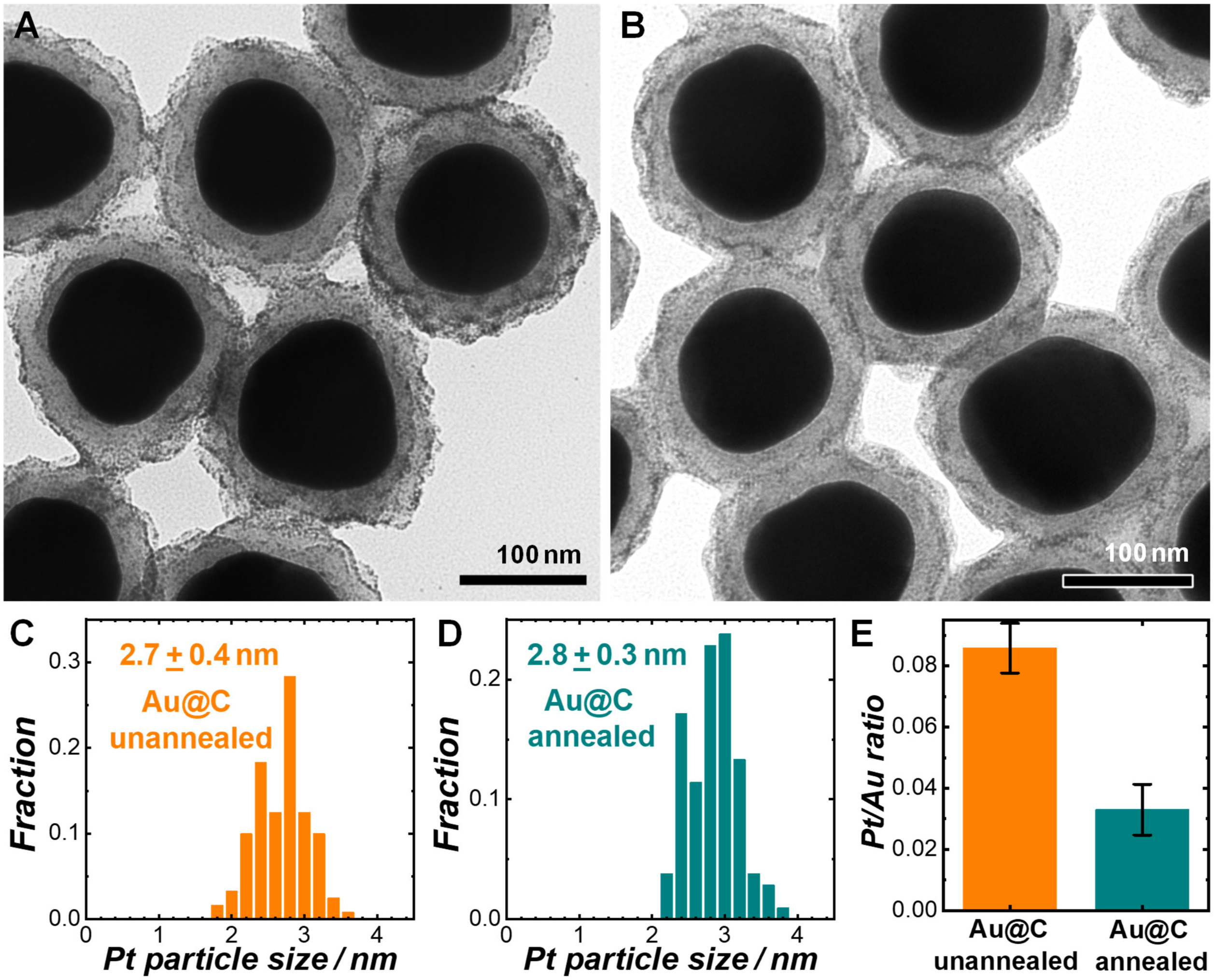

Figure S12. TEM images of Au@C/Pt nanohybrids synthesized by reacting (A) unannealed and (B) pre-annealed Au@C-3 (at 450 °C in an N_2 atmosphere for 2 h) with 300 µM of K_2PtCl_4. Distributions of Pt particle sizes deposited on the (C) unannealed Au@C-3 and (D) pre-annealed Au@C-3. (E) Pt/Au atomic ratios of Au@C/Pt nanohybrids synthesized by reacting unannealed and pre-annealed Au@C-3 with 300 µM of K_2PtCl_4.

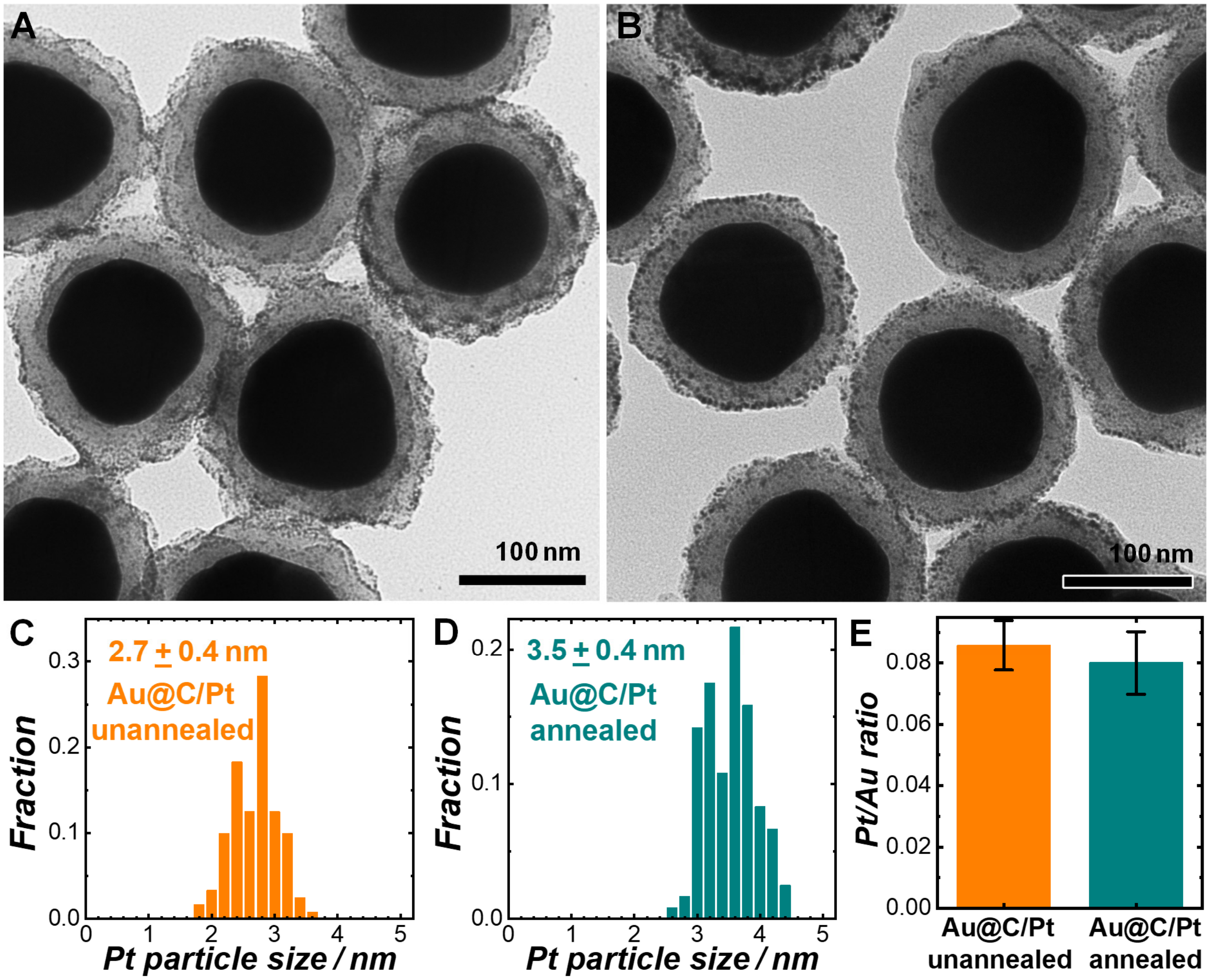

Figure S13. TEM images of (A) Au@C/Pt-6 (Au core size: 114 ± 6.3 nm; C shell thickness: 34.2 ± 3.8 nm; Pt/Au atomic ratio: 0.0858 ± 0.0081) and (B) Au@C/Pt-6 after thermal annealing at 450 °C in an N_2 atmosphere for 2 h. Distributions of Pt particle sizes for Au@C/Pt-6 (C) before and (D) after annealing. (E) Pt/Au atomic ratios (quantified by EDS) of Au@C/Pt-6 before and after annealing.

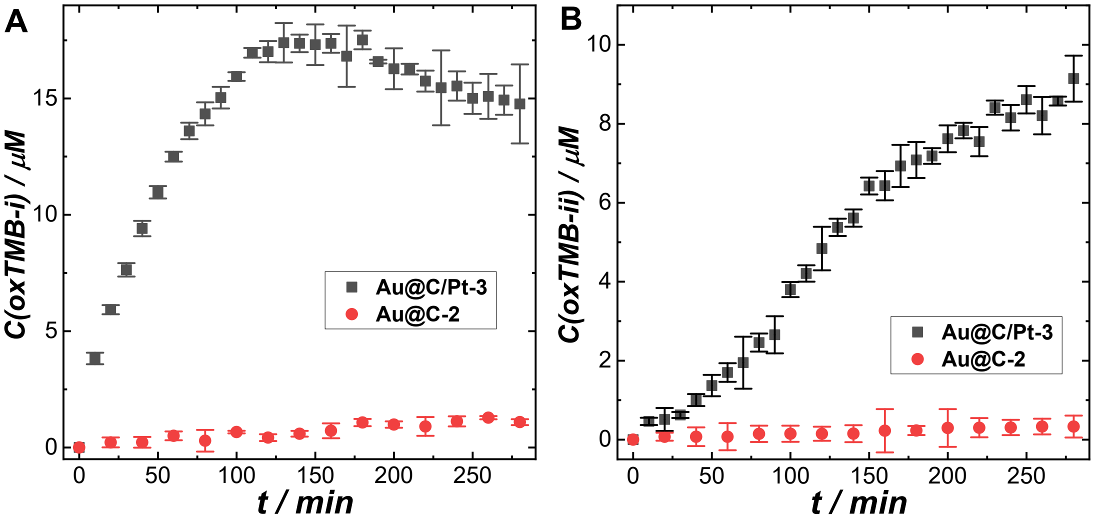

Figure S14. Temporal evolutions of (A) oxTMB-i and (B) oxTMB-ii concentrations during TMB oxidation reactions catalyzed by Au@C/Pt-3 (Au core size: 114 + 6.3 nm; C shell thickness: 20.4 + 2.4 nm; Pt/Au atomic ratio: 0.0526 + 0.0053) and Au@C-2 (Au core size: 114 + 6.3 nm; C shell thickness: 20.4 + 2.4 nm). The initial concentration of TMB was 100 µM. The pH of the reaction medium was 8. The reactions occurred at room temperature (25 ºC). Both Au@C/Pt-3 and Au@C-2 catalysts contained 2.33 µg Au. The total volume of the reactant mixtures was kept at 2.0 mL. The error bars represent the standard deviations of triplicate kinetic measurements under each reaction condition.

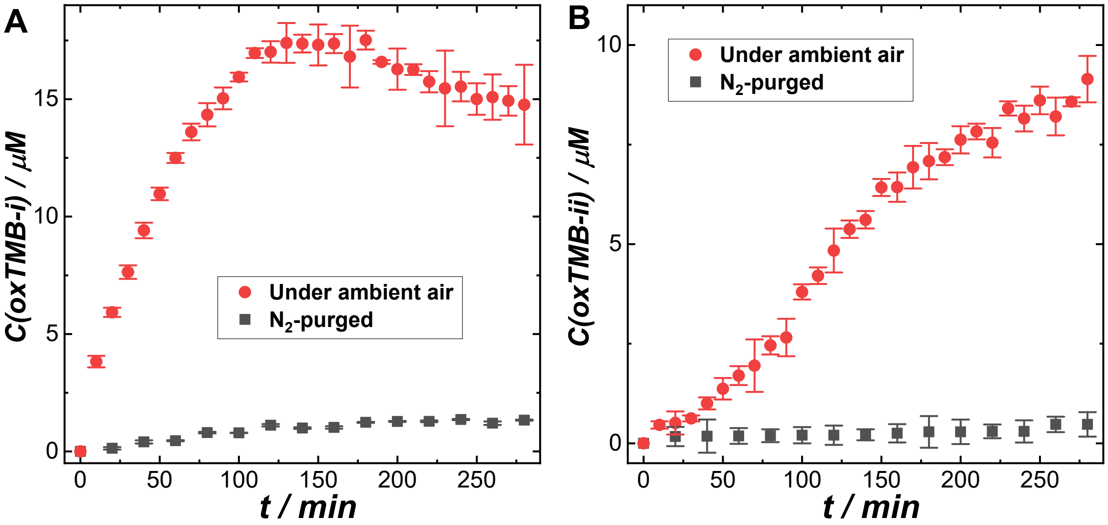

Figure S15. Temporal evolutions of (A) oxTMB-i and (B) oxTMB-ii concentrations during TMB oxidation reactions catalyzed by Au@C/Pt-3 under ambient air and in an N_2-purged reaction medium. The initial concentration of TMB was 100 µM. The pH of the reaction medium was 8. The reactions occurred at room temperature (25 ºC). The Au@C/Pt-3 catalysts contained 2.33 µg Au. The total volume of the reactant mixtures was kept at 2.0 mL. The error bars represent the standard deviations of triplicate kinetic measurements under each reaction condition.

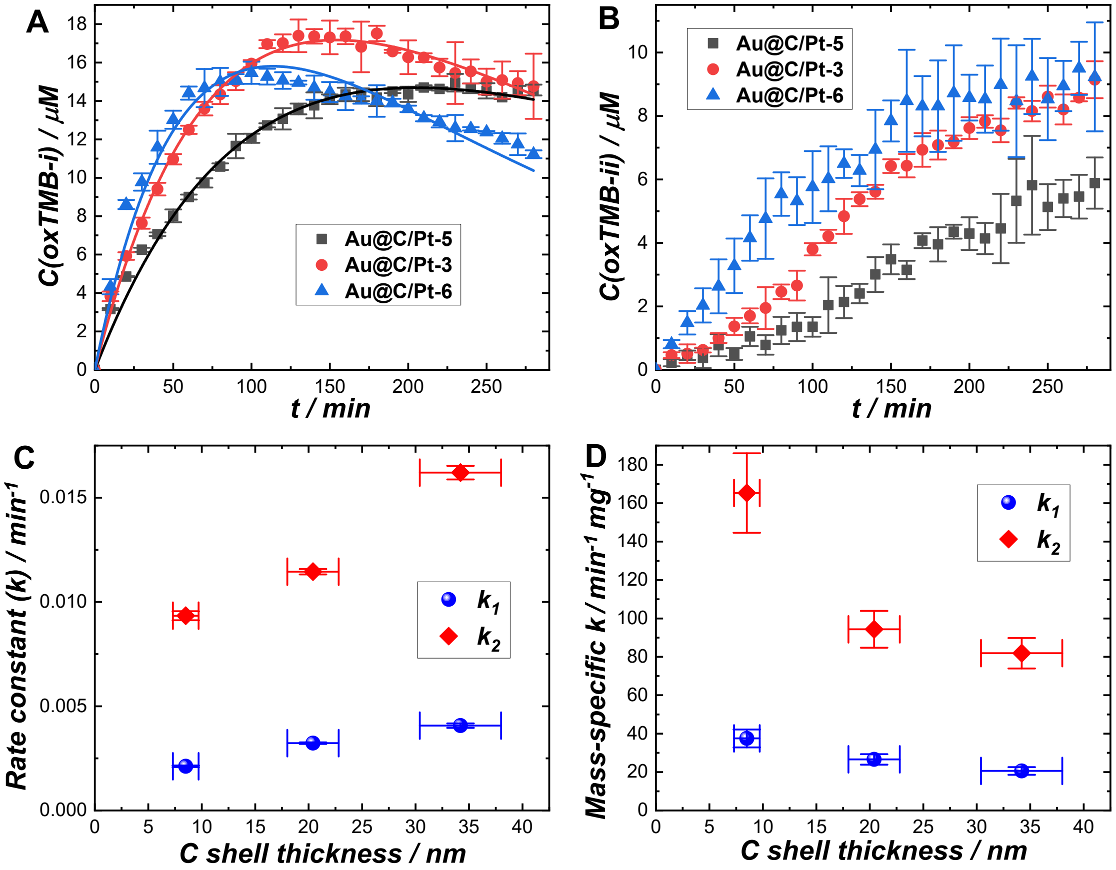

Figure S16. Temporal evolutions of (A) oxTMB-i and (B) oxTMB-ii concentrations during TMB oxidation reactions catalyzed by Au@C/Pt-5 (Au core size: 114 ± 6.3 nm; C shell thickness: 8.5 ± 1.2 nm; Pt/Au atomic ratio: 0.0245 ± 0.0030), Au@C/Pt-3 (Au core size: 114 ± 6.3 nm; C shell thickness: 20.4 ± 2.4 nm; Pt/Au atomic ratio: 0.0526 ± 0.0053), and Au@C/Pt-6 (Au core size: 114 ± 6.3 nm; C shell thickness: 34.2 ± 3.8 nm; Pt/Au atomic ratio: 0.0858 ± 0.0081). The initial concentration of TMB was 100 μM. The pH of the reaction medium was 8. The reactions occurred at room temperature (25 °C). The Au@C/Pt-3, Au@C/Pt-5, and Au@C/Pt-6 catalysts all contained 2.33 μg Au. The total volume of the reactant mixtures was kept at 2.0 mL. The error bars represent the standard deviations of triplicate kinetic measurements under each reaction condition. (C) Plots of apparent rate constants, k_1 and k_2, vs. C shell thickness. (D) Plots of mass-specific rate constants (k_1 and k_2 normalized against the Pt mass in the catalysts) *vs.* C shell thickness.

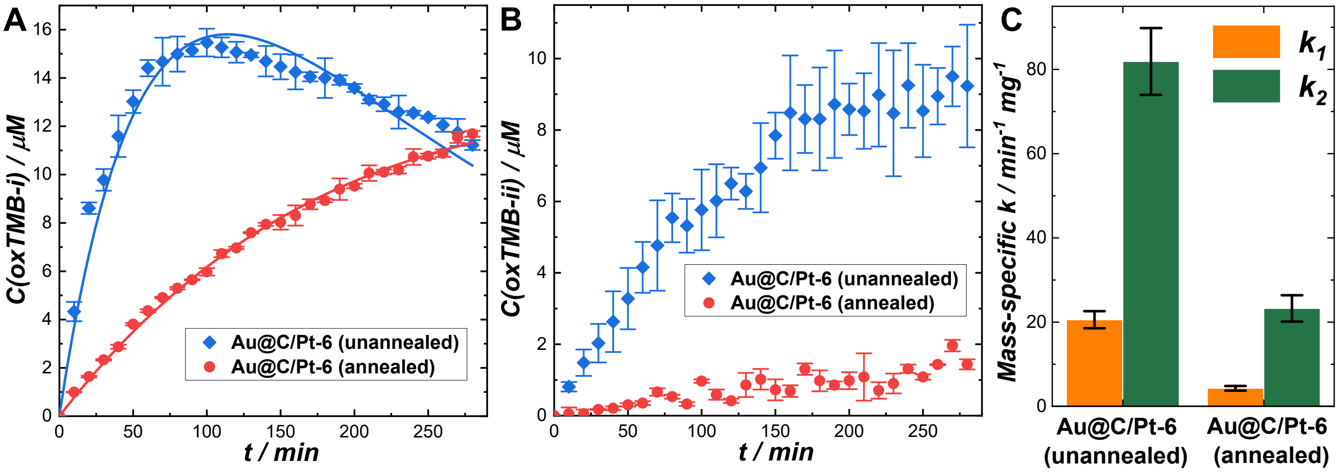

Figure S17. Temporal evolutions of (A) oxTMB-i and (B) oxTMB-ii concentrations during TMB oxidation reactions catalyzed by unannealed and annealed Au@C/Pt-6 (at 450 °C in an N_2 atmosphere for 2 h). The initial concentration of TMB was 100 μM. The pH of the reaction medium was 8. The reactions occurred at room temperature (25 °C). Both the unannealed and annealed Au@C/Pt-6 catalysts contained 2.33 μg Au. The total volume of the reactants mixtures was kept at 2.0 mL. The error bars represent the standard deviations of triplicate kinetic measurements under each reaction condition. (C) Pt mass-specific k_1 and k_2 of the reactions catalyzed by unannealed and annealed Au@C/Pt-6.

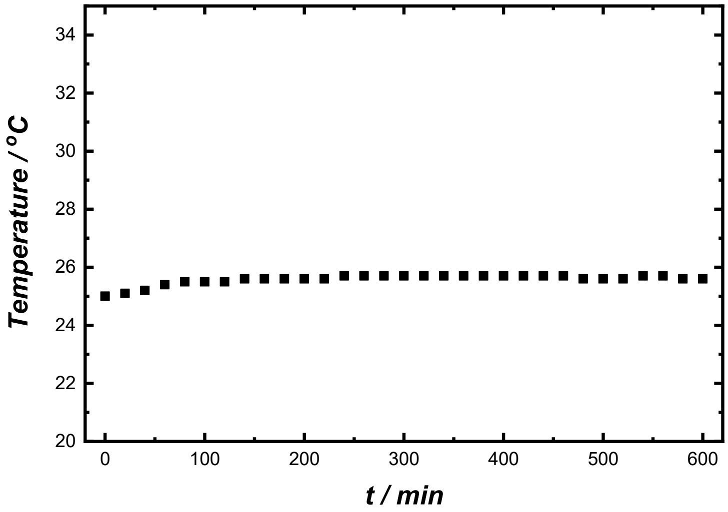

Figure S18. Temporal evolution of solution-phase temperature in a colloidal suspension of Au@C/Pt-3 under continuous illumination by a 638 nm laser (P_{ex}: 3.0 W) with temperature control using a circulating water bath. The total volume of the colloidal suspension was 2.0 mL, and the mass concentration of Au was 1.17 μg mL^{-1}.

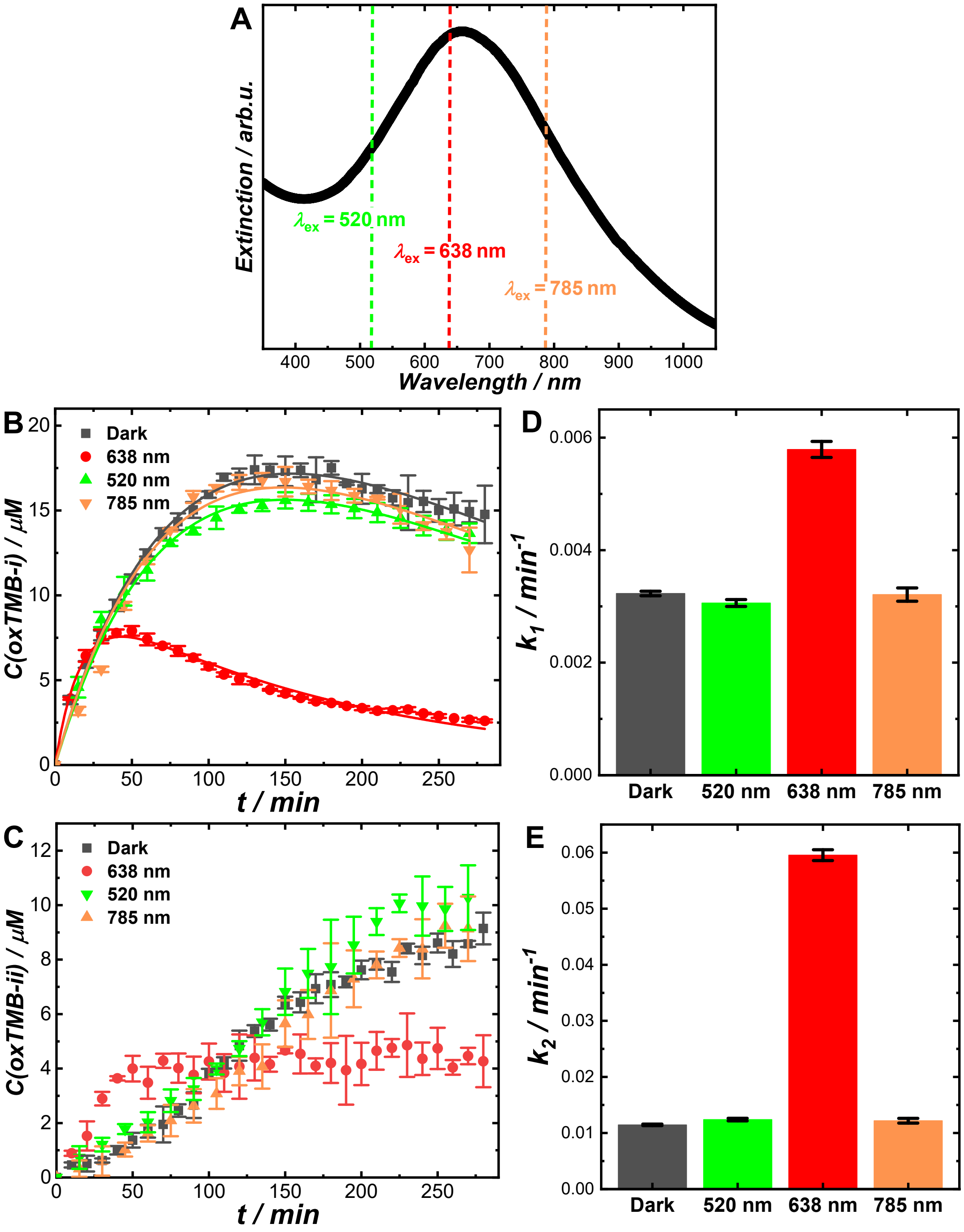

Figure S19. (A) Extinction spectrum of Au@C/Pt-3. The wavelengths of the excitation lasers were labeled with vertical dash lines. Temporal evolutions of (B) oxTMB-i and (C) oxTMB-ii concentrations during TMB oxidation reactions catalyzed by Au@C/Pt-3 in dark and under continuous illumination by the 520, 638, and 785 nm lasers at a P_{ex} of 3.0 W. The initial concentration of TMB was 100 µM. The pH of the reaction medium was 8. The reaction temperature was controlled at 25 ± 1 °C using a circulating water bath. The Au@C/Pt-3 catalysts contained 2.33 µg Au. The total volume of the reactant-catalyst mixtures was kept at 2.0 mL. The error bars represent the standard deviations of triplicate kinetic measurements under each reaction condition. (D) k_1 and (E) k_2 values of the reactions in dark and under continuous illumination by the 520, 638, and 785 nm lasers at a P_{ex} of 3.0 W.

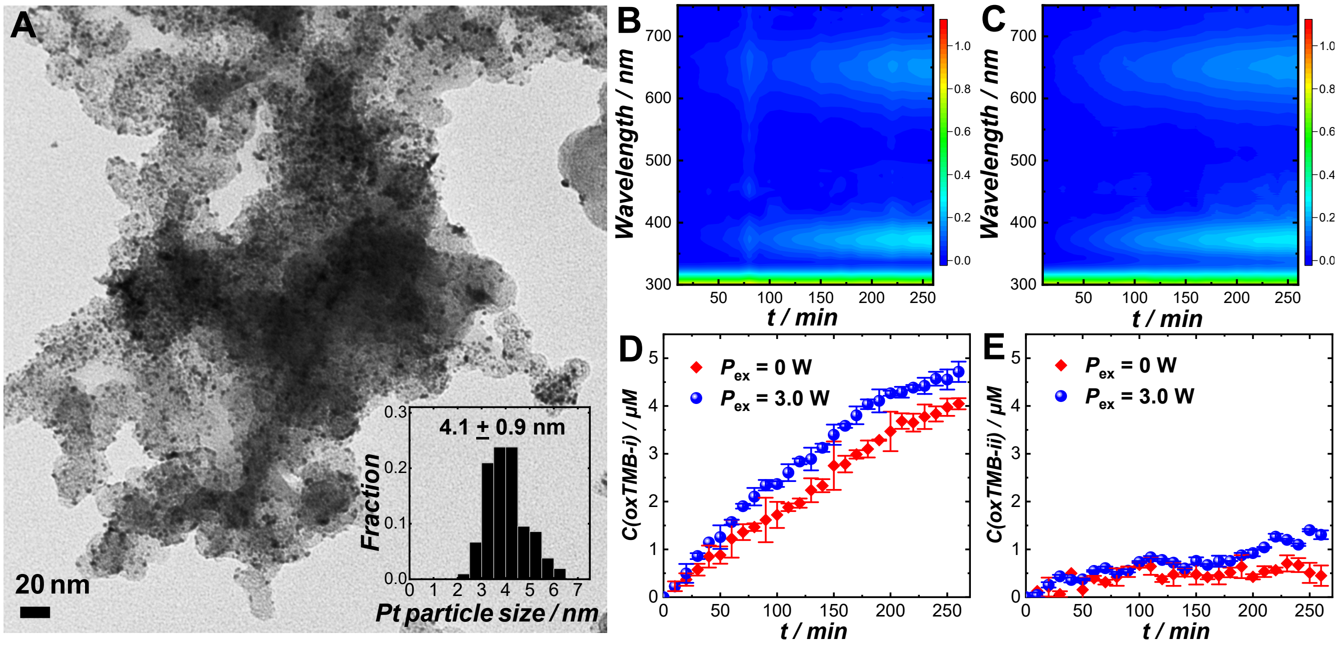

Figure S20. (A) TEM image of commercial Pt/C (20 wt % Pt). The size distribution of Pt nanoparticles in commercial Pt/C is shown in the inset panel. Temporal evolution of UV-vis absorption spectra during Pt/C-catalyzed TMB oxidation reactions (B) in dark and (C) under continuous laser illumination (λ_{ex}: 638 nm; P_{ex}: 3.0 W). Temporal evolutions of (D) oxTMB-i and (E) oxTMB-ii concentrations during Pt/C-catalyzed TMB oxidation reactions in dark and under continuous laser illumination (λ_{ex}: 638 nm; P_{ex}: 3.0 W). The initial concentration of TMB was 100 μM. The pH of the reaction medium was 8. The total volume of the reactant mixtures was kept at 2.0 mL. The Pt/C catalysts added to the reactant mixtures contained 0.12 μg of Pt. For the reaction occurring under laser illumination, the temperature was controlled at 25 ± 1 °C using a circulating water bath. The error bars represent the standard deviations of triplicate kinetic measurements under each reaction condition.

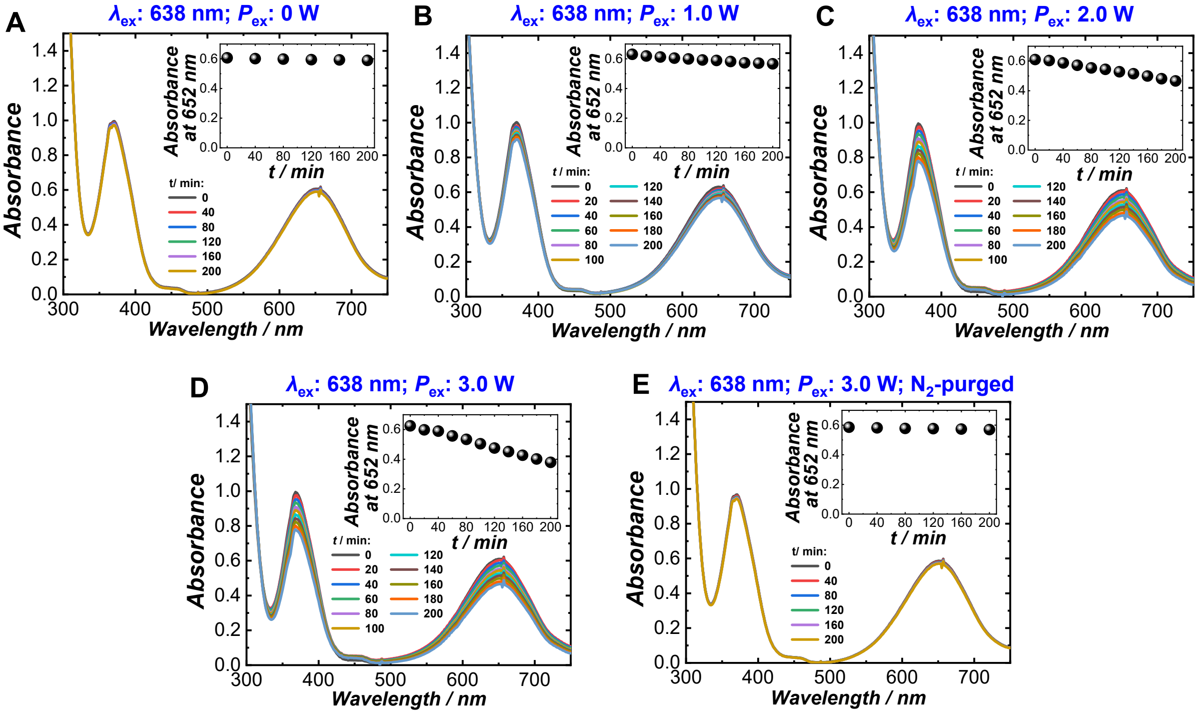

Figure S21. Temporally evolving UV-vis absorption spectra of oxTMB-i (A) in dark, under continuous laser illumination by a 638 nm laser at P_{ex}s of (B) 1.0, (C) 2.0, and (D) 3.0 W under ambient air, and (E) under continuous laser illumination (λ_{ex}: 638 nm; P_{ex}: 3.0 W) in an N_2-purged reaction medium. The inset panels show the temporal evolutions of the absorbance at 652 nm under each condition. oxTMB-i was produced through Au@C/Pt-3-catalyzed TMB oxidation reactions for 40 min. Then the Au@C/Pt-3 catalysts were separated from the reactant and product molecules through centrifugation. 2.0 mL of the oxTMB-i solution (pH of 8) was exposed to laser illumination with temperature control using a circulating water bath.

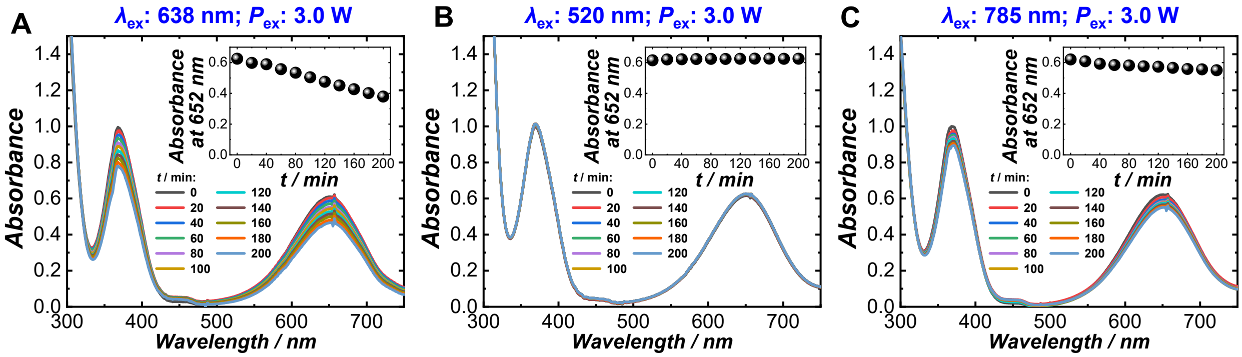

Figure S22. Temporally evolving UV-vis absorption spectra of oxTMB-i under continuous laser illumination at a P_{ex} of 3.0 W by a (A) 638 nm, (B) 520 nm, and (C) 785 nm laser. The inset panels show the temporal evolutions of the absorbance at 652 nm under each condition. oxTMB-i was produced through Au@C/Pt-3-catalyzed TMB oxidation reactions for 40 min. Then the Au@C/Pt-3 catalysts were separated from the reactant and product molecules through centrifugation. 2.0 mL of the oxTMB-i solution (pH of 8) was exposed to laser illumination with temperature control using a circulating water bath.

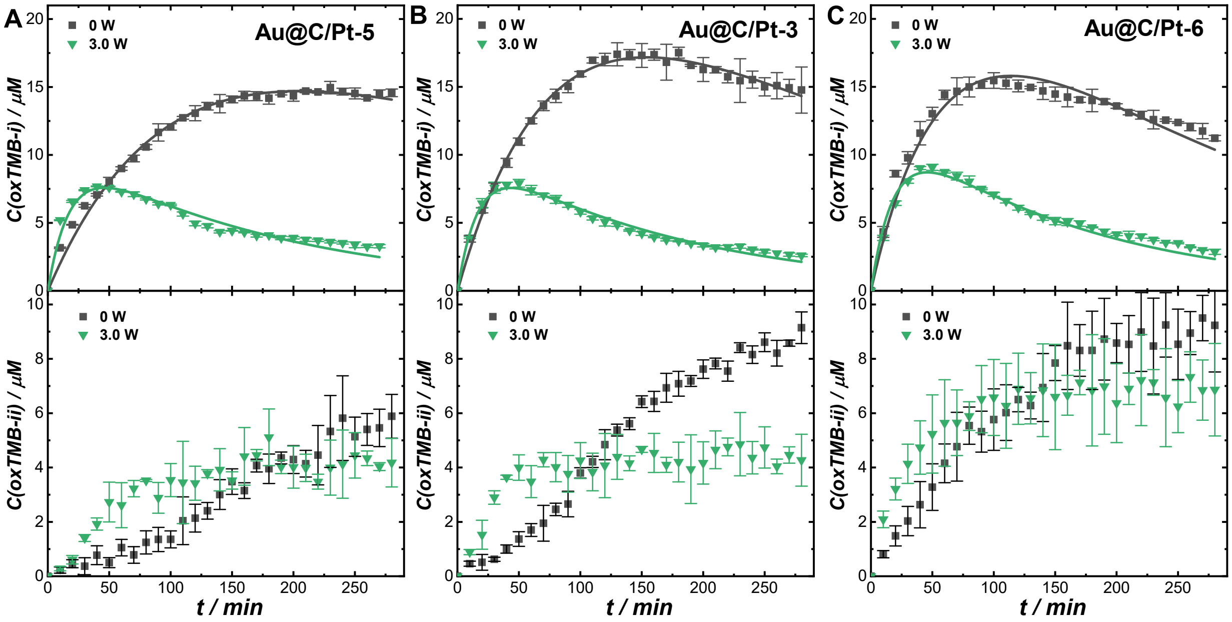

Figure S23. Temporal evolutions of oxTMB-i (upper panels) and oxTMB-ii (lower panels) concentrations during TMB oxidation reactions in dark and under continuous laser illumination (λ_{ex}: 638 nm; P_{ex}: 3.0 W) catalyzed by (A) Au@C/Pt-5, (B) Au@C/Pt-3, and (C) Au@C/Pt-6. The initial concentration of TMB was 100 μM. The pH of the reaction medium was 8. A circulating water bath was used to control the temperature at 25 ± 1 °C. The Au@C/Pt-3, Au@C/Pt-5, and Au@C/Pt-6 catalysts all contained 2.33 μg Au. The total volume of the reactant mixtures was kept at 2.0 mL. The error bars represent the standard deviations of triplicate kinetic measurements under each reaction condition.

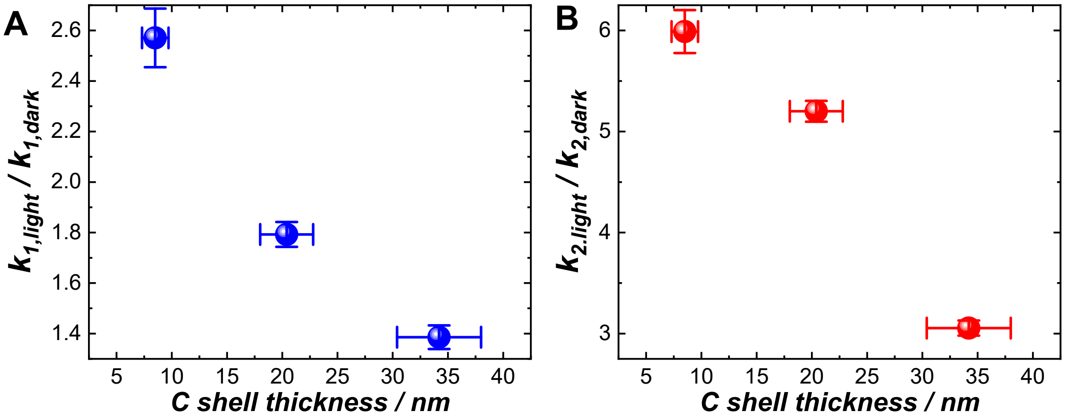

Figure S24. Relationship between photo-induced kinetic enhancements, defined as the ratios of the rate constants in dark and under laser illumination (λ_{ex}: 638 nm; P_{ex}: 3.0 W), and the thickness of C shells for (A) k_1 and (B) k_2. This figure shows the results of the comparative kinetic studies of the reactions catalyzed by Au@C/Pt-5, Au@C/Pt-3, and Au@C/Pt-6. The initial concentration of TMB was 100 μM. The pH of the reaction medium was 8. A circulating water bath was used to control the temperature at 25 ± 1 °C. The Au@C/Pt-3, Au@C/Pt-5, and Au@C/Pt-6 catalysts all contained 2.33 μg Au. The total volume of the reactant mixtures was kept at 2.0 mL.

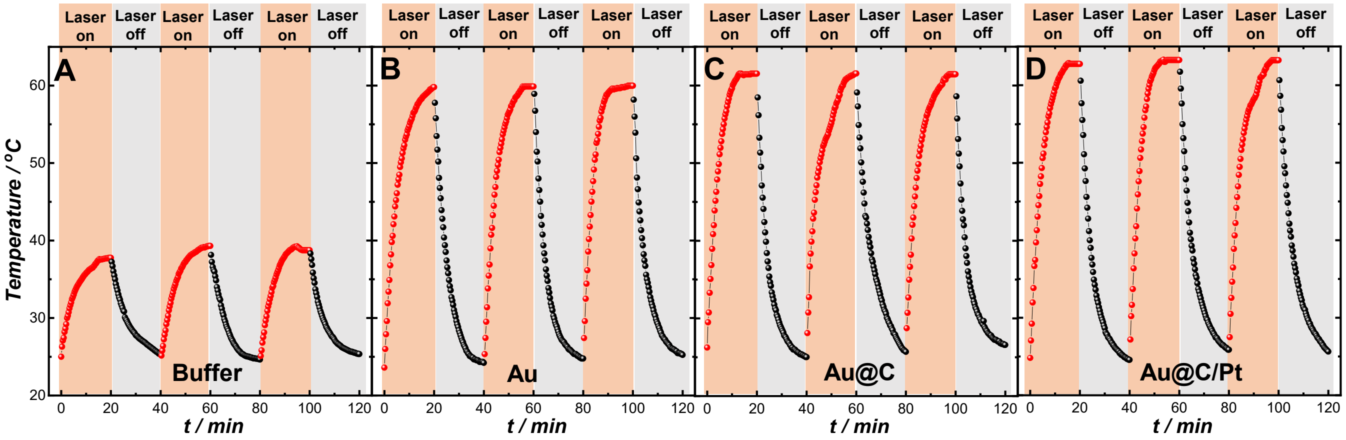

Figure S25. Temporal evolutions of solution-phase temperature in (A) a buffer solution (pH of 8), (B) colloidal Au nanoparticles (114 ± 6.3 nm), (C) colloidal Au@C-2 (Au core size: 114 ± 6.3 nm; C shell thickness: 20.4 ± 2.4 nm), and (C) colloidal Au@C/Pt-3 (Au core size: 114 ± 6.3 nm; C shell thickness: 20.4 ± 2.4 nm; Pt/Au atomic ratio: 0.0526 ± 0.0053) during three cycles of laser illumination (λ_{ex}: 638 nm; P_{ex}: 3.0 W) and cooling in dark under ambient air. For all samples used for the photothermal measurements, the total volume was 2.0 mL, and the mass concentration of Au was 1.17 μg mL^{-1}.

S3. References for Electronic Supplementary Information

1. P. N. Zhang, Y. J. Li, D. Y. Wang and H. B. Xia, High-Yield Production of Uniform Gold Nanoparticles with Sizes from 31 to 577 nm *via* One-Pot Seeded Growth and Size-Dependent SERS Property. *Part. Part. Syst. Charact.*, 2016, **33** (12), 924-932.

2. G. G. Li, D. A. Blom, S. Pandey, R. J. Koch, S. T. Misture, S. R. Phillpot and H. Wang, Overcoming the Interfacial Lattice Mismatch: Geometry Control of Gold-Nickel Bimetallic Heteronanostructures. *Part. Part. Syst. Charact.*, 2018, **35** (5), 1700361.

3. E. C. Cho, J. Xie, P. A. Wurm and Y. Xia, Understanding the Role of Surface Charges in Cellular Adsorption Versus Internalization by Selectively Removing Gold Nanoparticles on the Cell Surface with a I_2/KI Etchant. *Nano Lett.*, 2009, **9** (3), 1080-1084.